JMEPEG (2022) 31:3234–3248
https://doi.org/10.1007/s11665-021-06403-x

1059-9495/$19.00

Studies on Microstructure and Mechanical Properties of Weldments Produced in 12 mm Thick Naval Grade High Strength Low Alloy Steel for Sub-Zero Application by Single and Double Pass Hybrid Laser Arc Welding

M. Venkatesh Kannan, N. Arivazhagan, M. Nageswara Rao, G. Madhusudhan Reddy, K.V. Phani Prabhakar, and Padmanmabham Gadhe

Submitted: 1 June 2021 / Revised: 9 September 2021 / Accepted: 8 October 2021 / Published online: 15 November 2021

The present study deals with studies on HLAW joints produced in a naval grade HSLA steel using both single-pass (HLAW-1) and two-pass (HLAW-2) approach. The weld joints were subjected to different methods of characterization—optical microscopy, EBSD analysis, residual stress analysis, and mechanical testing. Microhardness testing, tensile testing and impact testing constituted the mechanical testing. Impact testing was carried out at both room temperature and − 60 °C. For both HLAW-1 and HLAW-2, the fusion zone and heat-affected zone (HAZ) showed higher hardness than the base metal and tensile fracture location was in the base metal. The HLAW-2 joint was characterized by a higher volume fraction of acicular ferrite, a higher fraction of high angle grain boundaries, and a finer grain size compared to the HLAW-1 joint. It is believed that these factors contributed to the observed higher impact toughness of the HLAW-2 joint at − 60 °C.

Keywords hybrid laser arc welding, impact toughness, naval grade HSLA steel, shipbuilding, sub-zero temperatures

1. Introduction

A high-strength low alloy (HSLA) steel, DMR 249A, was developed for strategic applications by defense metallurgical research laboratory (DMRL) for the Indian Navy. It possesses extremely high strength, as well as superior resistance to brittle fracture. The large size of this material in thicknesses ranging from 3.15 to 40 mm is essential for shipbuilding applications (Ref 1-3). Welding of thick plates of high strength low alloy (HSLA) steel for applications involving service at sub-zero temperatures is a challenging task. Of particular concern in such instances is the impact toughness of weld joints at −60 °C. In this context, hybrid laser arc welding (HLAW) has shown promise. While many studies were carried out with single-pass HLAW, some researchers also investigated two-pass HLAW (Ref 4-13). Different types of fusion welding processes can be adopted to weld naval grade HSLA steels. However, multi-pass welding is needed to weld high-thickness plates for shipbuilding applications (Ref 2, 3). In the meantime, while welding thick plates using conventional multi-pass welding, problems such as hot cracking, an excessive amount of residual stress, fatigue damage, distortion, and hydrogen-induced cracking in the weld were experienced due to non-uniform heating and cooling (Ref 14-16).

In order to avoid such problems, careful selection of suitable welding techniques and process parameters is important for welding thick plates of naval grade steels. In this context, a recently developed HLAW holds potential for welding thick plates of DMR 249A. Laser-GMA-hybrid welding process holds promise for welding of thick plates of DMR 249A. Since this process does not involve multi-pass melting, one can ensure uniform weld composition and hence, superior metallurgical and mechanical properties of the weldment. The advantage was attributed to faster cooling rate and smaller volume of weld metal associated with hybrid welding. Interactions of the two kinds of heat resources in hybrid welding enable to stabilize the welding arc and enlarge the scope of laser welding applications. With hybrid welding the product performance is improved; additionally, the production cost comes down and the productivity increases. This method of welding gives higher impact toughness than the other methods tried out in the published literature, and this is very vital to the use of the steel in the form of welded structures. The HLAW is categorized as low heat input, high depth of penetration, and high-speed welding process. Furthermore, the process is less demanding on the joint fit-up. Since multiple melting does not involve in this process, one can reckon that the weld composition would be consistent with superior metallurgical and mechanical properties of the weldment. To achieve high productivity in welding of HSLA steel in thick sections up to 25 mm, single-pass HLAW was studied by several researchers (Ref 17-20). Single-pass HLAW was also developed for successful welding of thick plates of maraging

M. Venkatesh Kannan, N. Arivazhagan, and **M. Nageswara Rao**, School of Mechanical Engineering, Vellore Institute of Technology, Vellore 632014, India; **G. Madhusudhan Reddy**, Metal Joining Group, Defence Metallurgical Research Laboratory, Hyderabad, India; and **K.V. Phani Prabhakar** and **Padmanmabham Gadhe**, International Advanced Research Centre for Powder Metallurgy & New Materials (ARCI), Balapur, Hyderabad, India. Contact e-mail: narivazhagan@vit.ac.in.

steel, reduced activation of ferritic martensitic steel for atomic energy application, and mild steel (Ref 21-23).

However, the weld root is narrow in HLAW; this leads to rapid cooling, eventually resulting in the formation of more martensite (Ref 24, 25). Even though martensite is found to be advantageous in obtaining high strength, the presence of a high volume of martensite leads to brittle failure during impact loading at low temperatures. An important requirement for naval grade steel is a minimum impact toughness of 78 joules at − 60 °C (Ref 1). High martensite formation can be efficiently avoided by implementing a slow cooling rate and preheating. The problems associated with narrow weld roots and fast cooling can be avoided by applying an additional pass of HLAW (Ref 17, 24, 25). There is no published literature on HLAW of DMR249A. To bridge this gap, single-pass (HLAW-1) and double-pass (HLAW-2) hybrid laser arc welding of DMR 249-A was investigated in the present study. The weldments produced by the two methods were compared with reference to metallurgical aspects and mechanical properties, particularly impact toughness at − 60 °C.

2. Experimental Procedure

Base material DMR 249A was procured in the form of a 14 mm thick plate. It was finely milled to realize plates with dimensions 100 × 300 × 12 mm^3. The HLAW process for 12 mm thick naval grade material DMR 249-A was developed at the International Advanced Research Centre for Powder Metallurgy and New Materials (ARCI) with their laser hybrid welding system comprising of Rofin DC035 slab CO_2 laser and Kemmpi synergic pulsed MIG/MAG. The laser beam is positioned normal to the workpiece, and the GMAW torch is positioned at an angle of 45° to the laser beam. The laser power of 3.5 kW is applied to the joint with a focused spot diameter of 180 μm. Prior to welding, bead on plate trials was performed to establish the optimum process parameters. Two pairs of plates, with dimensions as mentioned above, are employed to produce single-pass and double-pass HLAW butt joints. Schematic representation of the hybrid laser-arc welding is shown in Fig. 1. The edge preparation for both types of welding involved Y-type groove. However, the included angle for single-pass was 16° and for double-pass 40°. The schematic weld bead of single and double pass with butt joint configuration is shown in Fig. 2(a) and (b). The studies reported at references (Ref 21-23) for welding of thick steel plates formed the basis for the choice of parameters adopted in the present research.

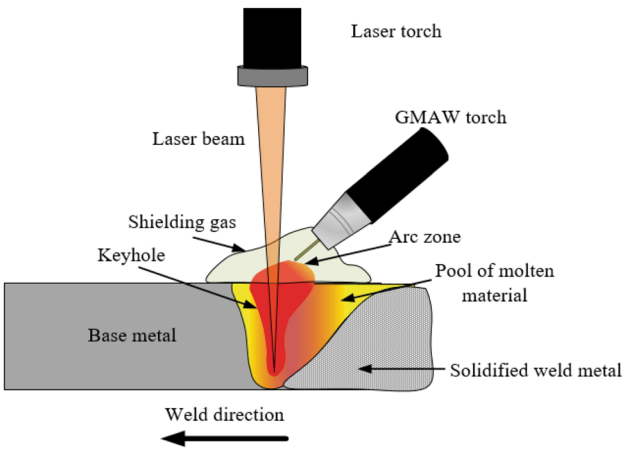

Fig. 1 Schematic representation of hybrid laser arc welding

The abutting surfaces of the plates were rubbed with an emery sheet and cleaned with acetone to ensure freedom of these surfaces from debris, residual oxide layer and grease. The plates were clamped rigidly for welding. The photographs of weldments fabricated by single-pass (HLAW-1) and double-pass (HLAW-2) are shown in Fig. 2(c) and (d), respectively. The filler material used in the study is 1.2 mm dia. ER80-Ni2; it is designed to promote acicular ferrite in the weld metal and realize a good combination of strength and toughness of the weld joints. The welded plates were tested using radiography to ensure that the weldment is defect-free. The chemical composition of base and filler metal was determined using optical emission spectroscopy (OES) and the results are shown in Table 1. The other process parameters used for single and double-pass welding are presented in Table 2. Subsequently, the plates were sliced using a wire electrical discharge machining (WEDM) process to realize test specimens as per ASTM standards as shown in Fig. 3(a) to carry out different tests.

Schematic representation of test coupons sliced for tensile, impact and residual stress analysis of both weldments is given in Fig. 3(b), (c) and (d), respectively. Sections perpendicular to the welding direction were extracted from the weldment and used for macro-examination, microstructure analysis, and microhardness. The residual stress analysis was carried out on the cap-side surface of the weldment, perpendicular to the weld direction. Prior to stress measurement, the samples were electrolytically polished to remove the layer affected by machining. Portable x-ray residual stress analyzer (Make: Pulstec Industrial Co., Ltd., Model: μ-X360n) was used to measure residual stresses. The working principle (cos α) and applicability of the analysis to weldments is discussed by previous researchers (Ref 24). The operating voltage was set at 30 kV and the target current at 1.0 mA. The target material in x-ray tube was chromium and the incident angle was pre-set to 35°.

The macro-examination was carried out with the help of a Dyno-lite AM4115T Edge digital microscope coupled with dinocapture software. The ZEISS Axio Lab.A1 optical microscope was used to perform the microstructural analysis. For the Fractography analysis, the fracture surface was examined by using Scanning Electron Microscope (Model and Make: Zeiss EVO 18) equipped with an EDS attachment. The EBSD analysis was made using Quanta™ 3D FEG; sample preparation for EBSD was made using the conventional emery polishing method up to 1500 grit emery sheet followed by electro-polishing with 80% methanol + 20% perchloric acid at 18 V for 20 seconds. The specimen was placed at a working distance of 12 mm with a tilt angle of 70° as discussed in previous research (Ref 26).

Microhardness was measured by using Vickers hardness tester (Make: M/S MATSUZAWA and Model: MMT-X). Hardness test was carried out on the cut samples of size 10mm × 12mm × 25mm. The load of 500g and dwell time of 10s was used. Hardness measurements were taken across the weld at three levels perpendicular to weld thickness, representing the cap, center, and root. The line at the cap is 1 mm away from the surface of the weldment, and the center line is 6 mm from the surface and the line at the root of the weldment is 11

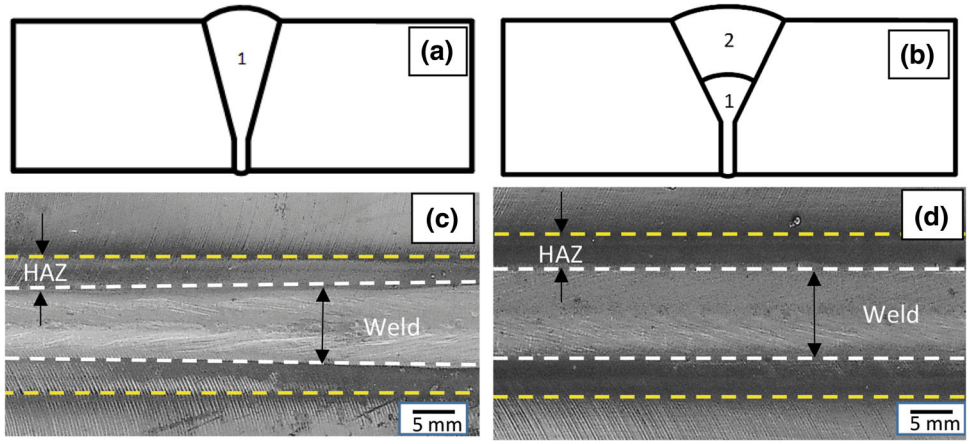

Fig. 2 Schematic representation of joint configuration for (a) single pass and (b) double pass. As-welded photographs of (c) single pass and (d) double pass

Table 1 Chemical composition of base metal and filler materials used

Wt.%	C	Mn	Si	P	S	Ni	Cr	Mo	V	Cu	Al	Nb	Ti	Pb	Sn	Fe
BM	0.08	1.4	0.24	0.01	0.013	0.7	0.026	0.006	0.04	0.15	0.05	0.04	0.013	0.001	0.001	Bal.
ER 80S-Ni 2	0.12	1.25	0.6	0.025	0.025	2.1	0.15	0.35	0.05	0.35	0.02	…	0.01	…	…	Bal.

Table 2 Process parameters

Process	Number of passes	Laser power	Arc Voltage, V	Current, A	Shielding gas flow rate (He), L/min	Heat input, KJ/mm	Wire feed rate, m/min
HLAW-1	1	3.5 kW	35	309	15	0.88	12
HLAW-2	1	3.5 kW	39	300	15	0.94	12
	2	0.7 kW	31	219	15	0.55	8

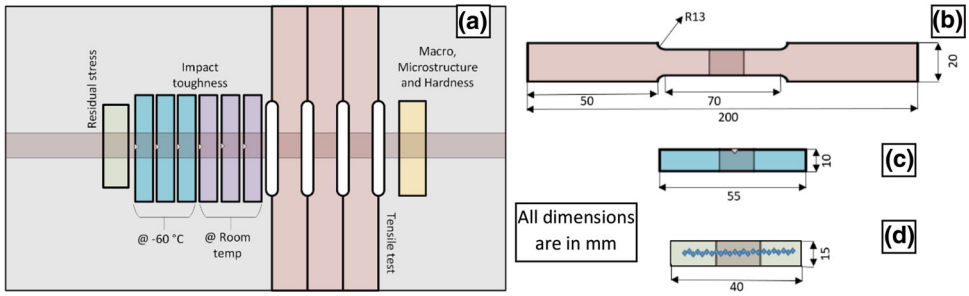

Fig. 3 Schematic representation of (a) The cut section of weldment for analysis (b) Tensile specimen (c) Impact specimen (d) Residual stress specimen

mm from the surface. Hardness measurement was carried out at an interval of 0.25 mm.

The tensile samples were prepared in accordance with ASTM E8/E8M. Tensile test is conducted by using a universal testing machine (Model: Instron 8801). Six Charpy V-notch blanks with dimensions 55 × 10 × 10 mm were sliced from each weldment. The blanks were etched to reveal the weld bead, prior to V-notch machining. The notch was machined at the middle of the weld bead using a broaching machine with a 45° angled cutting tool. Impact testing was carried out as per ASTM E23-07aε1. Tensile tests and impact tests were performed in triplicate to ensure repeatability. Impact test performed at room temperature and − 60 °C. In order to prepare

for the worst-case scenario in service, the lower test temperature of − 60° was chosen (Ref 25).

3. Results and Discussion

3.1 Macro- and Microstructure

The macrostructure at 10X magnification imaged at adjacent locations and stitched manually is shown in Fig. 4(a) (HLAW-1) and Fig. 4(b) (HLAW-2). The cross-section of the weldments produced using single pass and double pass shows full penetration. The weld bead has a wine cup shape, with a wide MIG zone at the upper side and the narrow laser zone on the lower side. The arc dominant zones and laser dominant zones are differentiated in the figures; arc dominant zones are indicated with discontinuous lines and laser dominant zones with continuous lines. The wine-shaped weld bead is common when HLAW is carried out [21, 23]. It can be seen from Fig. 4 that the weld seam is higher in the case of HLAW-2. The bead width at the weld center and root is higher in the case of HLAW-2.

In Fig. 5 and 6, the different zones in the composite weldment are matched with the corresponding regimes of the Fe-C phase diagram for HLAW-1 and HLAW-2, respectively (Ref 27). In addition, the different parts of the heat-affected zone are delineated in the figures. It was seen that there was no significant difference between the overall widths of the heat-affected zone (HAZ) in the two welds. As one moves from the fusion zone, a partially melted zone with a small thickness occurs first, as seen in Fig. 5 and 6. The coarse-grained HAZ occurs next. The partially melted zone got dark etched, possibly due to relatively high heat input.

Figure 7 shows optical microscopic images of different locations of the HLAW-1 weld joint. Fig. 7(a) shows the microstructure of the base material; it consists of polygonal ferrite. Fig. 7(b) shows the microstructure of fine grain HAZ; Fig. 7(c) shows the microstructure of coarse-grained HAZ fusion zone interface. Fig. 7(d)-(f) shows the microstructures of the cap, center and root regions of the fusion zone, respectively. The microstructural constituents seen in the fusion zone include acicular ferrite, bainite, grain boundary ferrite and Widmanstatten ferrite. Microstructure is not the same at the cap, center and root locations of the fusion zone. For example, the cap region contains substantially more acicular ferrite compared to center region. Figure 7(e) shows the prior austenite grain boundaries. It has been shown that the prior austenite grain size is a function of the total heat input during the weld thermal cycle. The prior austenite grain size plays an important role in defining the microstructural scale of low-temperature phases and the mechanical properties (e.g., strength, ductility, fracture toughness, etc.) of steels in the final product form. The prior austenitic grain boundaries are mostly high-angle grain boundaries and are considered as an advantageous in increasing ductile to the brittle transition temperature. The presence of prior austenite grain boundaries helps in blunting the crack growth across the grains. Influence of HLA weld process parameters on prior austenite grain size and its effect of this grain size on specific mechanical properties of weld joints can be the subject of more detailed and systematic study. As brought out by Beata Bialobrzeska et al. (Ref 28), revealing the prior austenite grain boundaries is a difficult task. Influence of HLA weld process parameters on prior austenite grain size and the effect of this grain size on specific mechanical properties of weld joints can be the subject of more detailed and systematic study.

Figure 8 shows optical microscopic images of different locations of the HLAW-2 weld joint. Figure 8(a) shows the microstructure of HAZ-fusion zone interface region. Figure 8(b), (c) and (d) shows the microstructures of cap, centre and root regions of the fusion zone, respectively. The microstructural constituents are the same as those seen in the fusion zone of HLAW-1. However, there are differences in the volume fractions. For example, there is a higher fraction of acicular ferrite in center region of HLAW-2, compared to HLAW-1.

As stated in the "Experimental Procedure" section, the filler wire is designed to promote acicular ferrite in the microstructure. The substantial amount of acicular ferrite seen in the microstructures of both HLAW-1 and HLAW-2 is a testimony to it. The filler wire contains higher levels of Ni, Mo, Cr, Si, C, and Cu compared to the base metal. The effect of several of these elements in terms of promoting acicular ferrite in the microstructure is documented in the literature. For example, Zhang et al. brought out that a higher amount of Ni in C-Mn-Ni weld metals results in higher amount of acicular ferrite in the microstructure (Ref 29). Tang et al. reported an increase in acicular ferrite with increasing Mo level in microalloyed low carbon line pipe steels (Ref 30). Lee et al. demonstrated that increasing Cr level in low carbon steel welds increases the volume fraction of acicular ferrite in the weld metal microstructure (Ref 31). Higher Si level is expected to promote higher count of silica type inclusions, thereby enhancing the volume fraction of acicular ferrite. It is well established that nucleation of acicular ferrite is favored by non-metallic inclusions in steel (Ref 32-34).

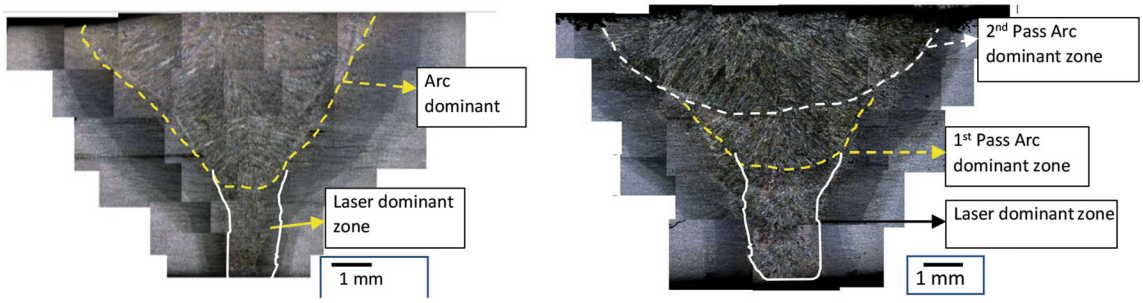

Fig. 4 Stitched image of macrostructure at 10X (a), HLAW-1 (b) HLAW-2

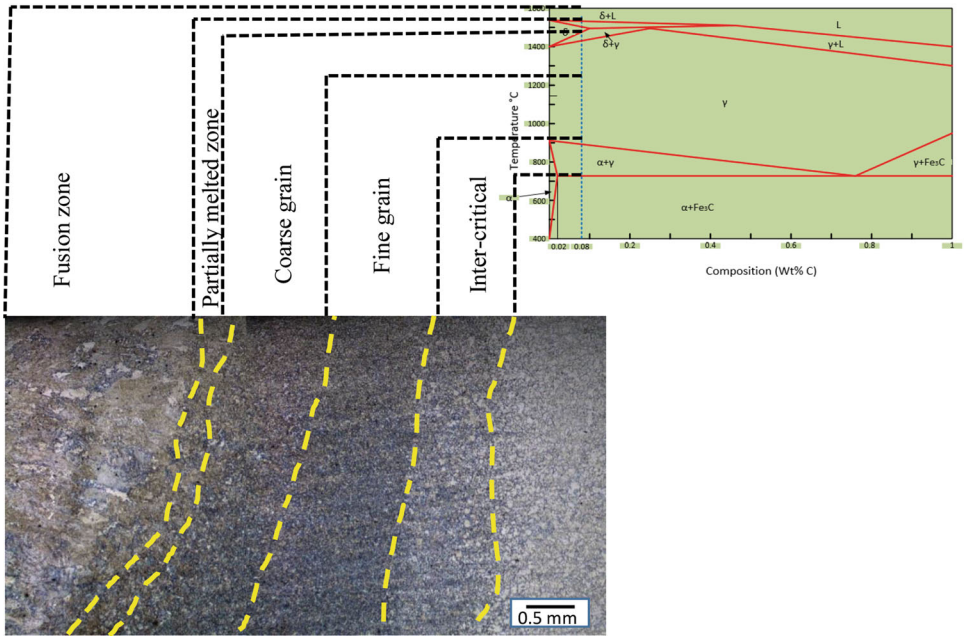

Fig. 5 The evolution of different microstructure in single pass hybrid laser arc welding

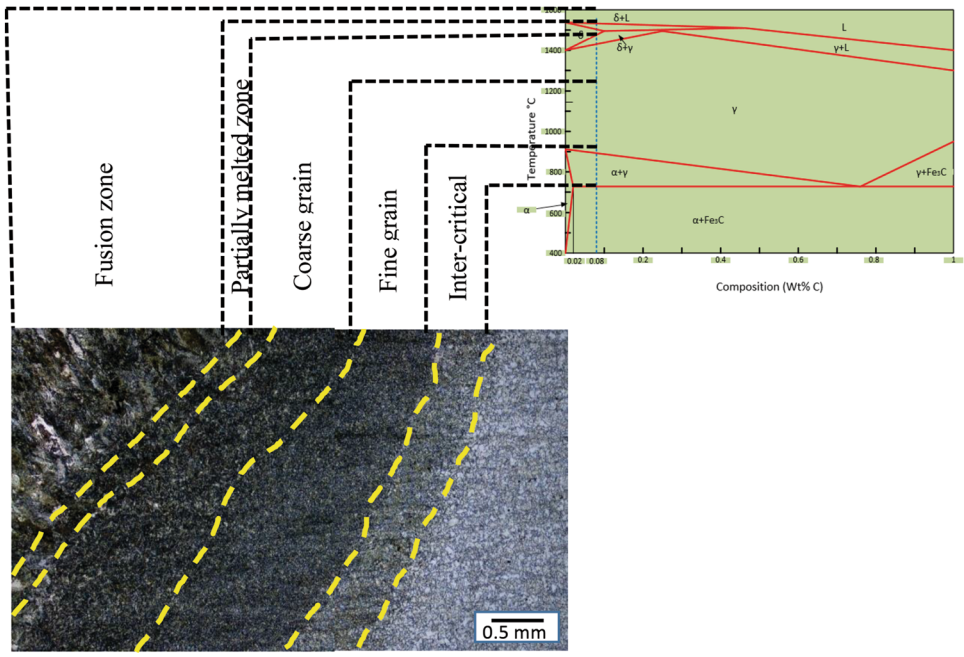

Fig. 6 The evolution of different microstructure in double pass hybrid laser arc welding

3.2 Electron Backscattered Diffraction Analysis

The electron backscattered diffraction (EBSD) analysis was carried out on the center location of the fusion zone for both HLAW-1 and HLAW-2. The results are presented in Fig. 9(a)-(d). Figure 9(a) and (b) shows the inverse pole figure analysis for HLAW-1 and HLAW-2, respectively. The grain misorientation analysis is shown in Fig. 9(c) and (d) for the two weld joints. Classification is made among the boundaries, depending on whether the misorientation angle is 2° to 5°, 5° to 15° or >15°. If the misorientation angle is 2° to 5°, it is a manifestation of dislocation tangles within the grains. If the angle is in the range 5° to 15°, they are low-angle grain boundaries. Boundaries with angle > 15° are considered as high-angle grain boundaries. From the EBSD analysis presented in Fig. 9, it is seen that HLAW-1 has 51.6 % high-angle grain boundaries and HLAW-2 60.2 % such boundaries. In other words, HLAW-2 has a higher fraction of high-angle grain boundaries. These high-angle grain boundaries resist crack propagation, thereby contributing to higher toughness. The subject is discussed further in the impact testing section later in this article. EBSD studies at the center location also showed that the grain size of the HLAW-2 fusion zone (1.37 μm) is finer than that of HLAW-1 (2.07 μm) (Table 3).

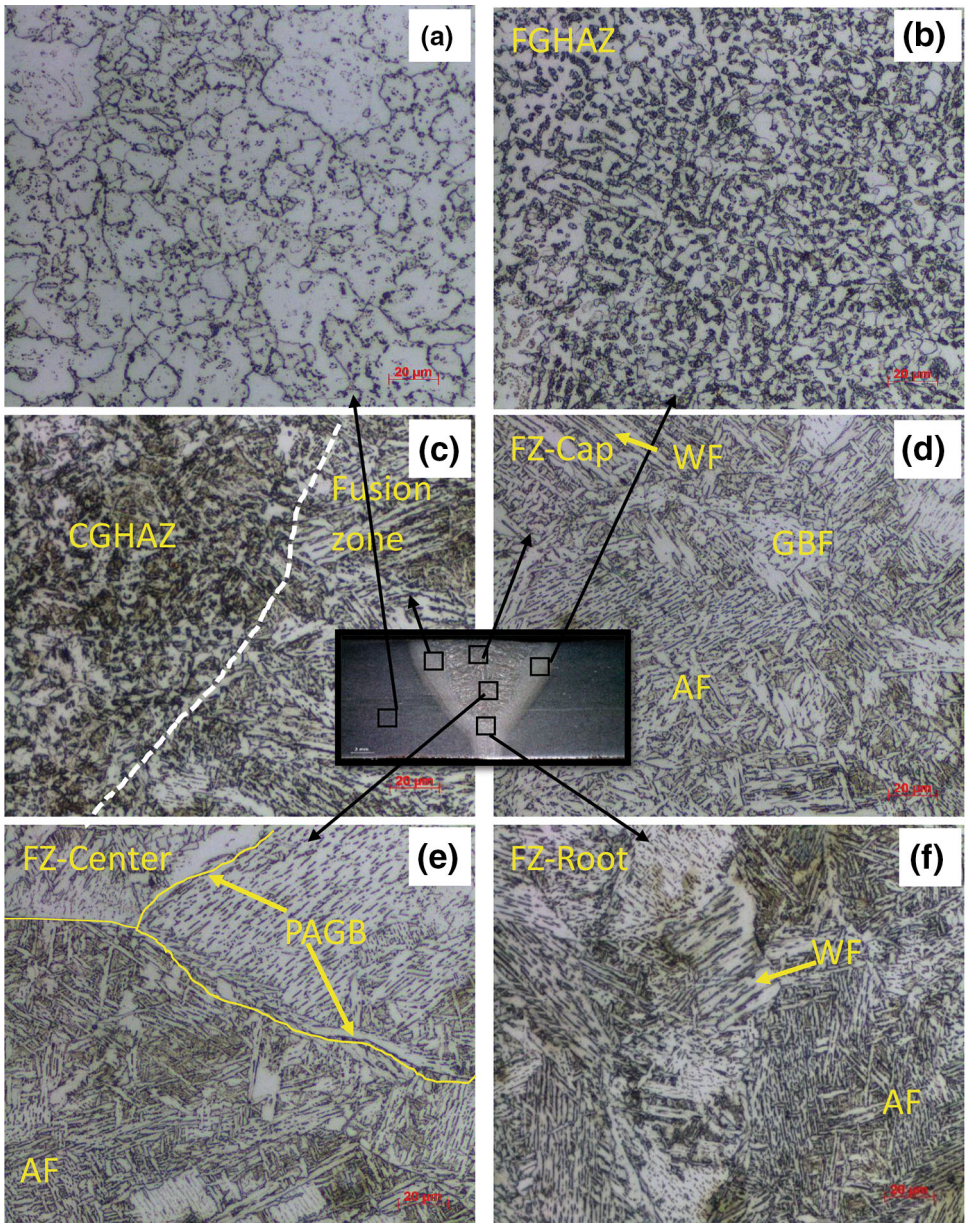

Fig. 7 Microstructure HLAW-1 (a) BM (b) FGHAZ (c) CGHAZ-FZ interface (d) FZ cap (e) FZ center (f) FZ root. AF:acicular ferrite, WF:Widmanstatten ferrite, PAGB:prior austenitic grain boundary, GBF:grain boundary ferrite

3.2.1 Distortion and Residual Stress Measurement. Angular distortion of HLAW-1 and HLAW-2 weldments was evaluated with a coordinate measuring machine. HLAW-1 showed a distortion of 0.2°, while the distortion for HLAW-2 was 0.3°. The total heat input in HLAW-1 was 887.3 J/mm, the corresponding value for HLAW-2 was 1585.7 J/mm. The higher angular distortion of HLAW-2 can be attributed to the higher heat input involved.

Residual stress was measured on the cap-side surface. Measurements were carried out on both sides of the weldment. Figure 10 shows the residual stress profile for the two welds. The residual stress in the base material was found to be close to zero. Its value increases steadily and as one travels through HAZ. A maximum tensile residual stress level of 248 MPa is reached for HLAW-1 and 286 MPa for HLAW-2. On moving from the HAZ/fusion zone interface towards the centre of the fusion zone, there is a drop in tensile residual stress. A minimum is reached in the weld centre, the minimum value being 170 MPa for HLAW-1 and 142 MPa for HLAW-2. However, the maximum tensile stress levels are lower compared to those measured after SMAW and A GTAW (Ref 17) and this is an advantage from the safety point of view. The stress pattern was found to be symmetrical about the weld centre. The residual stress pattern was an M shape profile. Such profiles were obtained by Pamnani et al. in weldments produced in 10 mm thick plates of the same steel produced by activated flux gas tungsten arc welding and shielded metal arc welding (Ref 17). The authors attributed it to the occurrence of transformation products in the fusion zone- acicular ferrite, bainite and Widmanstatten ferrites forming by a displacive mechanism causing invariant plane strain with a large shear and grain boundary and polygonal ferrite forming by a volume change.

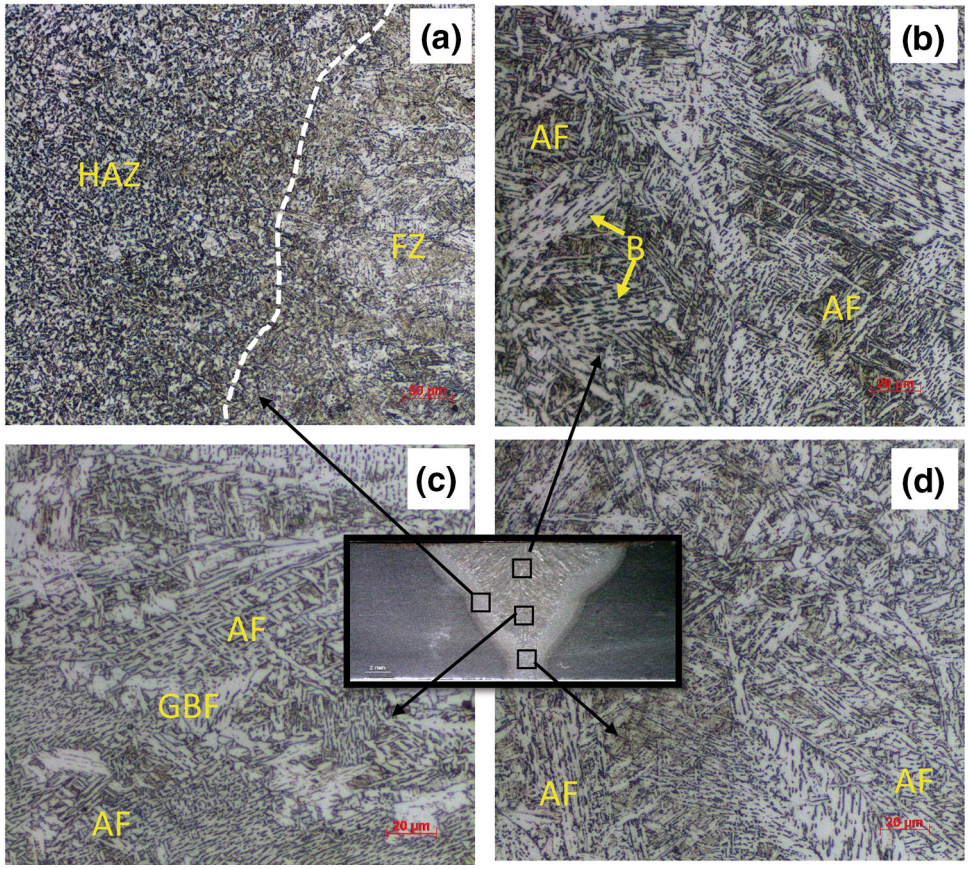

Fig. 8 Microstructure HLAW-2 (a) HAZ-FZ interface (b) FZ cap (c) FZ centre (d) FZ root. AF:acicular ferrite, WF:Widmanstatten ferrite, PAGB:prior austenitic grain boundary, GBF:grain boundary ferrite, B:bainite

3.3 Microhardness

Microhardness plots across the HLAW-1 and HLAW-2 weldments, covering fusion zone, HAZ, and base metal are shown in Fig. 11 and 12. The plot is symmetrical around the weld centre; hence only one side of the plot is given in the figures. Average values of hardness obtained in the fusion zone and HAZ at cap, centre and root of the two weldments are presented in Table 4. The base metal hardness was found to be in the range 165-175 Hv. For both weldments, there is a steep increase in hardness as one moves through HAZ towards the fusion zone. Thus, the hardness values of fusion zone are the highest. Hardness values of HAZ lie in the intermediate range. It is seen in Table 4 that in all the three locations (cap, center, root) microhardness values of HAZ are lower than those of the fusion zone. The microstructure of the base metal consists of polygonal ferrite, which is a soft phase. The fusion zone consists of a significant volume fraction of phases such as acicular ferrite, bainite, which are relatively hard phases.

It is also seen from Table 4, that the microhardness values of fusion zone are slightly higher for HLAW-2 than those for HLAW-1; this is true for all three locations (cap, center, root). A contribution to this may be coming from the relative grain size. EBSD studies at the centre location showed that grain size of the HLAW-2 fusion zone (1.37 μm) is finer than that of HLAW-1. Based on the Hall-Petch relationship, the hardness of HLAW-2 fusion zone should be higher, which is in line with the results obtained.

3.4 Tensile Tests

The results of tensile testing are presented in Fig. 13(a)-(d) for HLAW-1 and 14a-d for HLAW-2. Figure 13(a) and 14(a) shows the stress-strain curves. Photographs of specimens before testing and the three fractured specimens are given in Fig. 13(b) and 14(b). Photographs of the fracture surfaces taken at a low magnification are shown in Fig. 13(c) and 14(c). Photographs obtained with a high magnification are shown in Fig. 13(d) and 14(d). Table 5 summarizes the results of tensile testing for HLAW-1 and HLAW-2. It was seen that fractures in both cases occurred in the base metal, well away from HAZ. Table 5 shows that the strength and ductility values for HLAW-1 and HLAW-2 are comparable (99-100% efficiency). Further, the strength and ductility values of the two weldments match well with the corresponding values of the base metal. This is also consistent with the observation that fracture occurred in the base metal in both cases. It is predicted from the tensile results that variation in microstructure in different zones of the weldment influenced on the weld tensile behavior. By the comparison of single and double pass hybrid laser arc welding, the number of passes very much influenced on weld mechanical properties of the DMR 249 weldment. The microhardness plots shown in Fig. 11 and 12 for HLAW-1 and HLAW-2 show that the fusion zone is the hardest, HAZ has an intermediate hardness and base metal is the softest. This explains why fractures occurred in both cases in the base metal (Ref 35, 36). In line with the good ductility values of the two weldments (% elongation of 25 and 27 for HLAW-1 and HLAW-2, respec-

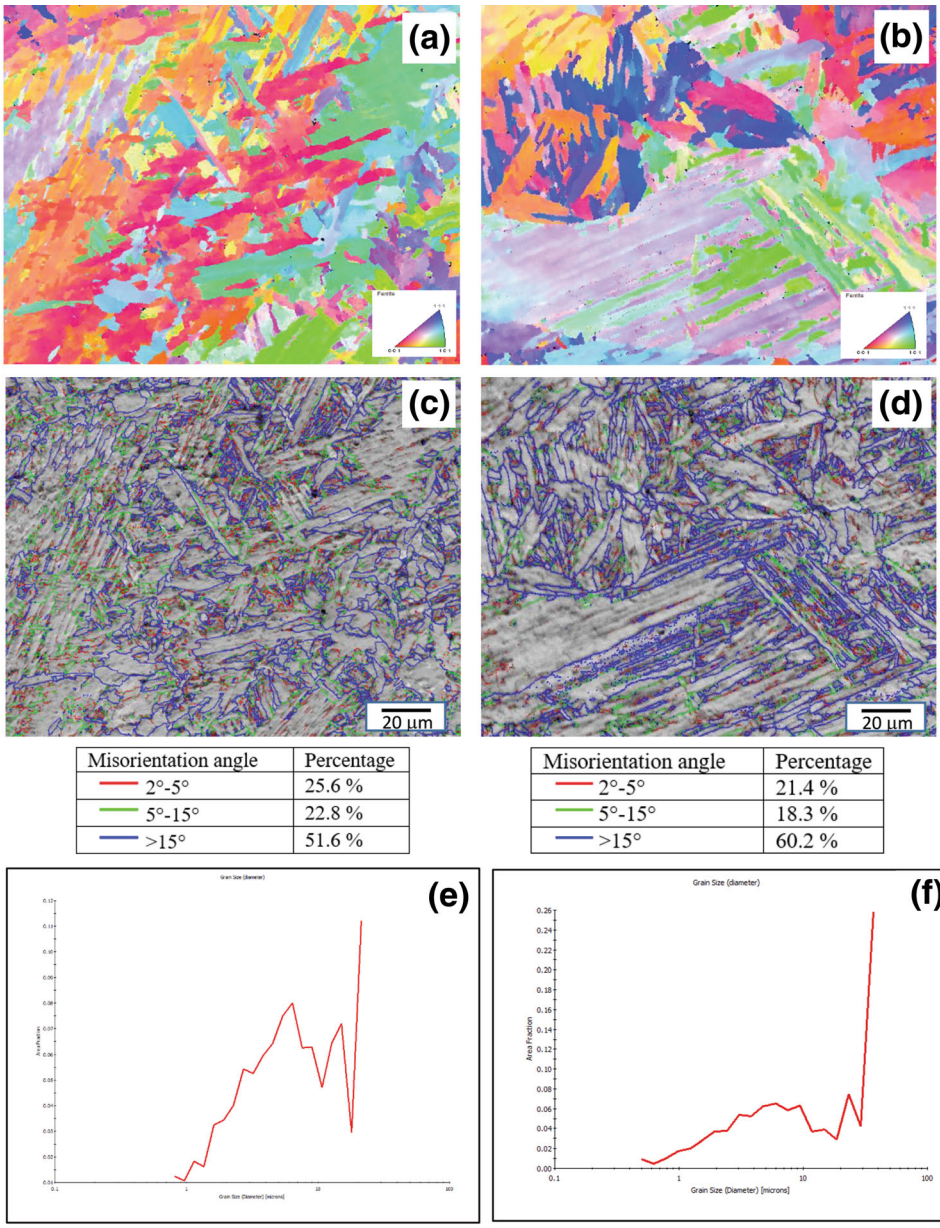

Fig. 9 EBSD analysis at FZ (a) Inverse pole figure of HLAW-1 (b) Inverse pole figure of HLAW-2 (c) Misorientation angle volume fraction HLAW-1 (d) Misorientation angle volume fraction HLAW -2, (e) Grain size analysis of HLAW-1 (f) Grain size analysis of HLAW-2

Table 3 Boundary density and grain size at the weld zone

Volume ratio				
Sample	**$<2°$**	**$>2°$ and $<15°$**	**$>15°$ and $<60°$**	**Grain size**
HLAW-1	8%	38%	54%	2.07
HLAW-2	6%	35%	59%	1.37

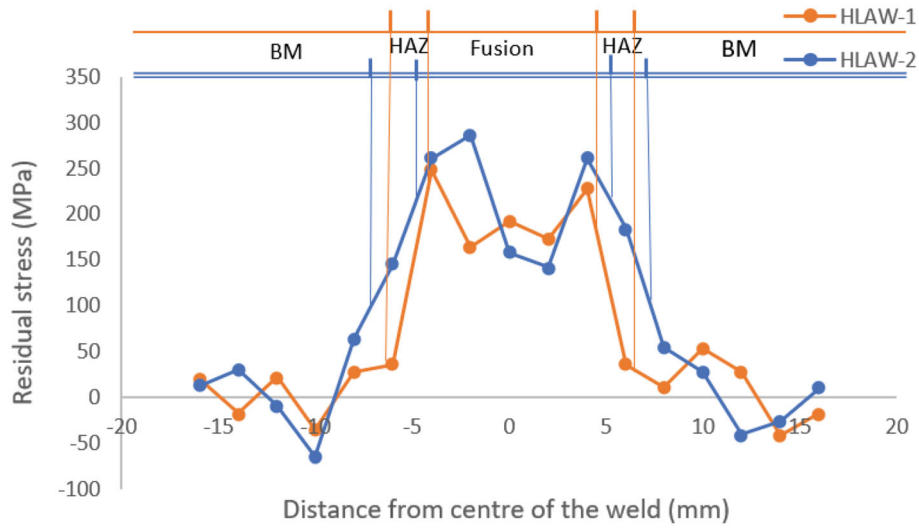

Fig. 10 Residual stress analysis of HLAW-1 and HLAW-2

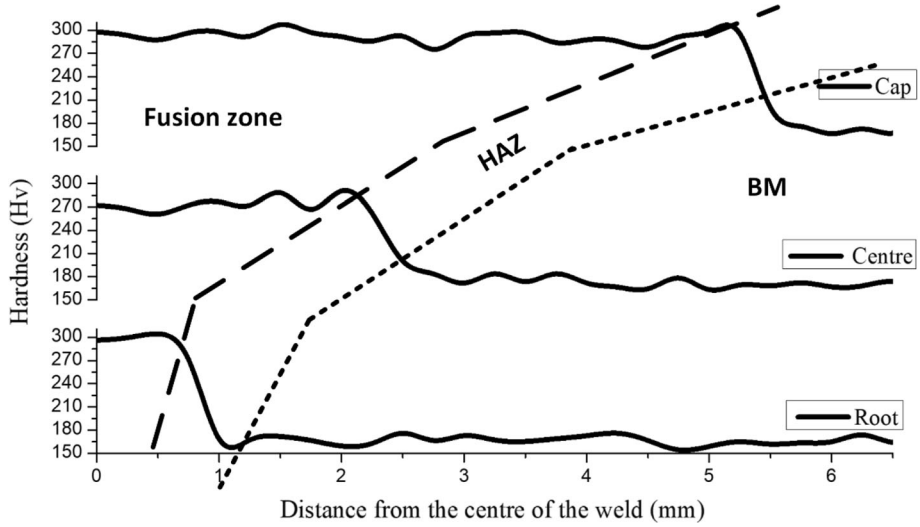

Fig. 11 Microhardness of HLAW-1

tively), their fracture surfaces at high magnification, shown in Fig. 13(d) and 14(d), demonstrate the presence of dimples all over.

3.5 Impact Toughness

Impact test results of HLAW-1 are presented in Fig. 15. Figure 15(a), (b) and (c) shows the results of room temperature testing. Figure 15(a) is the macroscopic side view of the broken impact specimen. Macroscopic top view of the broken specimen is given in Fig. 15(b). Figure 15(c) is a scanning electron microscopic image of fracture surface appearance at a magnification of 10,000X. Figure 15(d), (e) and (f) give corresponding images for impact testing at -60°, except that the magnification for fractograph in Fig. 15(f) is 2500X. The results of impact testing of HLAW-2 are presented in Fig. 16. Figure 16(a)-(c) covers the room temperature testing. Figure 16(a) and (b) shows the side view and top view of the broken impact specimen at a low magnification, while Fig. 16(c) presents the SEM picture of the fracture surface at high magnification (2500X). Figure 16(d), (e) and (f) shows corresponding images for impact testing at -60°, except that the magnification for fractograph in Fig. 16(f) is 2500X. The impact toughness values collected at room temperature and − 60 °C on the two weldments are included in Table 5. Impact toughness values of the base metal at the two test temperatures are also included in the Table to facilitate comparison. Base metal as well as the HLAW-1 and HLAW-2 show a drastic drop in toughness when test temperature is lowered from room temperature to − 60 °C. This is in line with the fractographic observations as shown in Fig. 15(c) and (f) for HLAW-1 and 16c and 16f for HLAW-2. Fracture occurs in a ductile manner at room temperature and fracture surface is dimpled in nature. At − 60 °C it is a mixed-mode of fracture; regions showing both ductile fracture and brittle fracture can be seen on the fracture surface.

HLAW-2 shows higher toughness at both room temperature and − 60 °C compared to HLAW-1. At − 60 °C, toughness of HLAW-2 (84 J) is 9 % higher than that of HLAW-1(75 J). There may be more than one contributing factor for the higher toughness of HLAW-2. For example, HLAW-2 has more

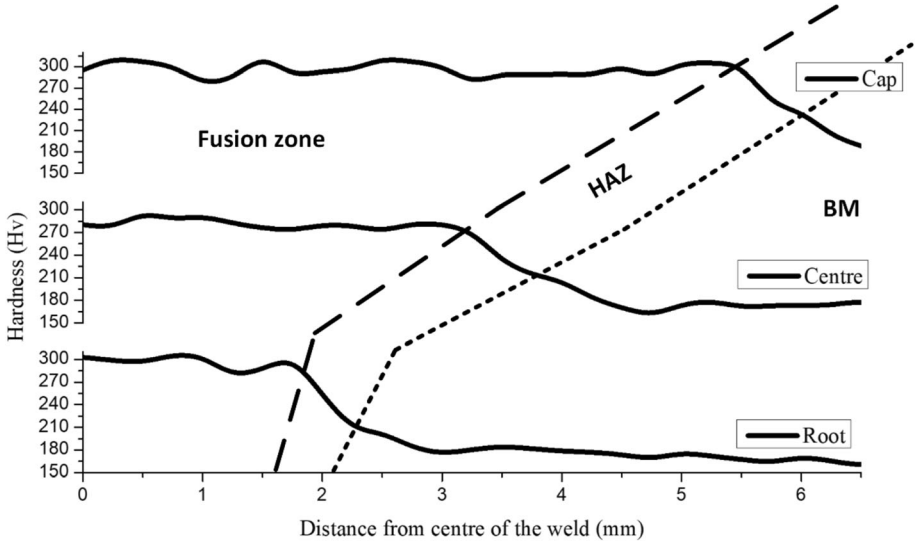

Fig. 12 Microhardness of HLAW-2

Table 4 Average hardness of different zones of the weldment

	HLAW-1, HV		HLAW-2, HV	
Line of test	**HAZ**	**Weld**	**HAZ**	**Weld**
Cap	247 ± 3.9	294 ± 6.6	263 ± 5.9	296 ± 5.4
Centre	250 ± 5.4	275 ± 7.3	255 ± 6.1	280 ± 6.2
Root	226 ± 4.5	292 ± 8.2	235 ± 3.4	298 ± 7.2

amount of acicular ferrite in the microstructure than HLAW-1. It is well documented that the more the interlocking acicular ferrite in the microstructure, the more is the toughness. EBSD studies brought out that HLAW-2 has a higher percentage of high angle grain boundaries. There are several studies (Ref 14, 15, 37-39) which established that high angle grain boundaries restrict the cleavage crack growth. Impact testing at − 60 °C includes fracture by cleavage and the higher percentage of high angle grain boundaries in HLAW-2 may be contributing to restrict the cleavage crack growth and enhance the impact toughness. Higher volume fraction of interlocking acicular

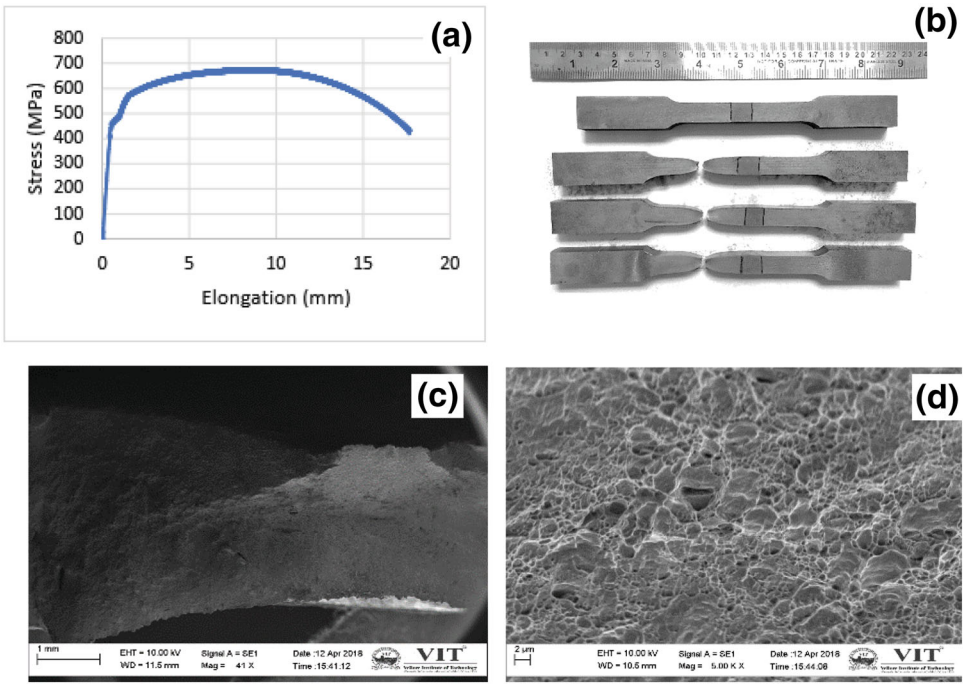

Fig. 13 (a) Stress elongation diagram (b) Tensile-tested specimen HLAW-1 (c) Fractography at 41X (d) Fractography at 5KX

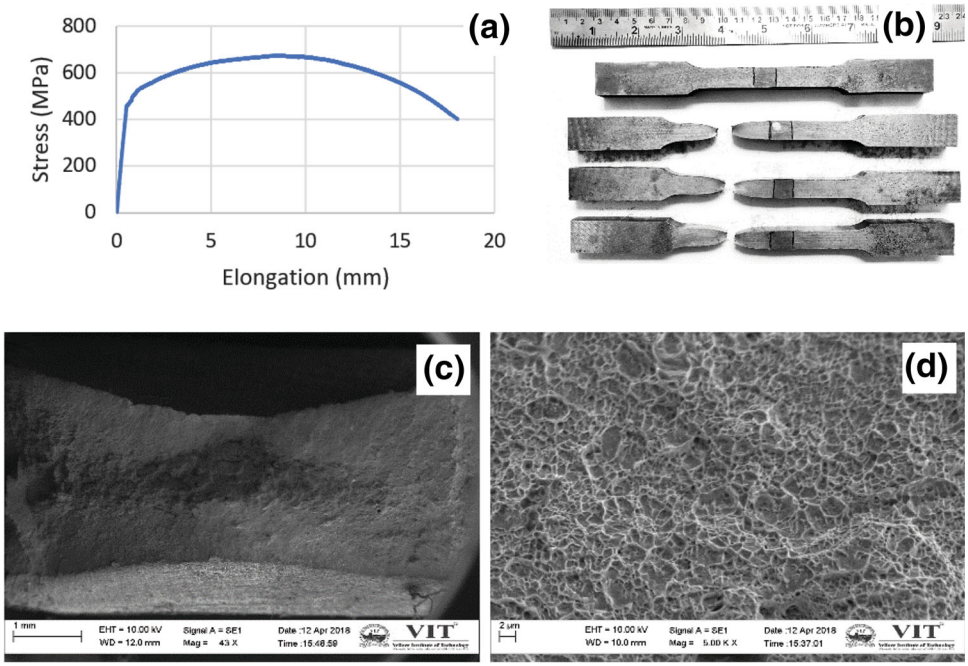

Fig. 14 (a) Stress elongation diagram (b) Tensile-tested specimen HLAW-2 (c) Fractography at 43X (d) Fractography at 5KX

Table 5 Mechanical properties of the weldment

		Welding of DMR 249-A using ER80S-Ni 2		
Tensile parameters	**Units**	**HLAW single pass**	**HLAW double pass**	**Base metal**
Ultimate tensile strength	MPa	682	694	683
Yield strength	MPa	451	458	469
Elongation %	%	25	27	28
Maximum load	kN	70	74	72
Fracture zone	…	BM	BM	…
V-Notch Charpy impact toughness at RT	J	196	244	260
V-Notch Charpy impact toughness at − 60 °C	J	75	84	96

ferrite and higher fraction of high-angle grain boundaries may not be totally independent factors. It has been documented that acicular ferrite has a higher density of high-angle grain boundaries (Ref 40). The grain size of the weld also influences the toughness. EBSD study showed that grain size is 2.07 μm and 1.37 μm in HLAW-1 and HLAW-2. Finer grain size may also be contributing to the higher toughness observed in HLAW-2. Here again, the grain size and fraction of interlocking acicular ferrite may not be totally independent factors. Acicular ferrite has a very fine grain size and the higher percentage of this ferrite variant in HLAW-2 might be contributing to the finer grain size, as measured by EBSD.

Details of the chemical composition of weld metals for HLAW-1 and HLAW-2 are shown in Table 6. The % C in HLAW- is 0.078, close to that of the base metal. The % C in HLAW-1 is 0.096%, slightly higher than that of base metal. It has been documented in the literature that increasing carbon % in the weld metal leads to decreasing toughness (Ref 39, 40). The lower %C may thus be contributing to the higher toughness of HLAW-2. The %Mn in HLAW-2 weld metal (1.4%) is higher than that in HLAW-1 weld metal (1.08 %). It has been reported that manganese promotes acicular ferrite at the expense of proeutectoid ferrite (Ref 41). The observed higher percentage of acicular ferrite in HLAW-2 might have had a contribution from the higher %Mn in this weldment. The minimum specified value for impact toughness of the base metal at − 60 °C is 78J. The weld joint is considered to be of acceptable quality when its toughness is ≥ 90% of that of base metal, i.e., ≥ 70 J. It thus emerged that both HLAW-1 and HLAW-2 gave acceptable results.

It may be pointed out that the sub-zero impact toughness values obtained by the HLAW-1 and HLAW-2 are higher than those reported by Pamnani et al. for weldments of 10 mm thick plates of the same steel produced by activated flux gas tungsten arc welding, submerged arc welding, and flux-cored arc welding (Ref 38). Further sub-zero impact toughness of HLAW-2 is higher than that reported by Pamnani et al. for shielded metal arc welding joints in 10 mm thick plates of the same steel (Ref 38). Thus HLAW-2 seems to be a promising method for the welding of DMR249A thick plates with strong toughness of sub-zero.

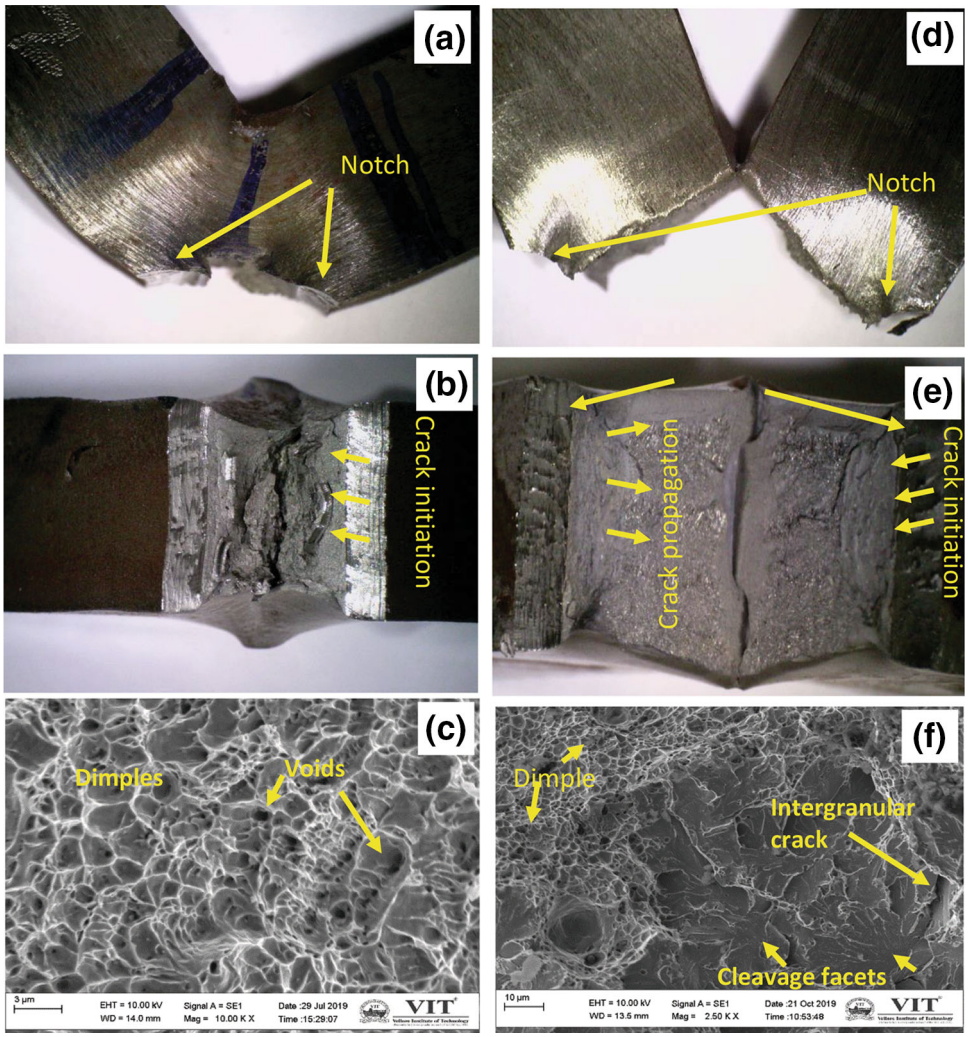

Fig. 15 Fracture impact tested HLAW-1 sample (a-c) at room temperature (d-f) at -60°C (a, c) Side view (b, e) Top view (c) Fractography at 10 KX (f) Fractography at 2.5KX.

4. Conclusions

The present research is about the comparative evaluation of weldment produced in thick plates of a naval grade high strength low alloy steel by single-pass and double-pass hybrid laser arc welding. The following conclusions could be reached.

1. Optical microscopy revealed the presence of acicular ferrite, bainite, grain boundary ferrite and Widmanstatten ferrite in the fusion zones of two weldments. HLAW-2 fusion zone consists of a higher amount of acicular ferrite than the fusion zone of HLAW-1.
2. EBSD analysis revealed (i) higher presence of high angle grain boundaries and (ii) finer grain sizes in HLAW-2 compared to HLAW-1.
3. The residual stresses developed in HLAW-1 and HLAW-2 were found to have an 'M' shaped profile. The development of this profile is attributed to the occurrence of acicular ferrite, Widmanstatten ferrite, grain boundary ferrite, and bainite in the fusion zone.
4. For both weldments microhardness in the fusion zone was the highest, the presence of martensite and acicular ferrite/bainitc ferrite contributing to the high hardness. HAZ had intermediate hardness, while the base metal with the soft polygonal ferrite microstructure had the lowest hardness.
5. Both welds fractured in the base metal region after tensile testing. This is because the base metal is softer than the fusion zone and HAZ.
6. HALW-2 showed 9% higher impact toughness at −60°C than HLAW-1. This is attributed to higher % acicular ferrite, higher % of high angle grain boundaries, and finer grain size in the HLAW-2 fusion zone.
7. Both HLAW-1 and HLAW-2 meet the specificational requirements of the naval steel in terms of sub-zero impact toughness.

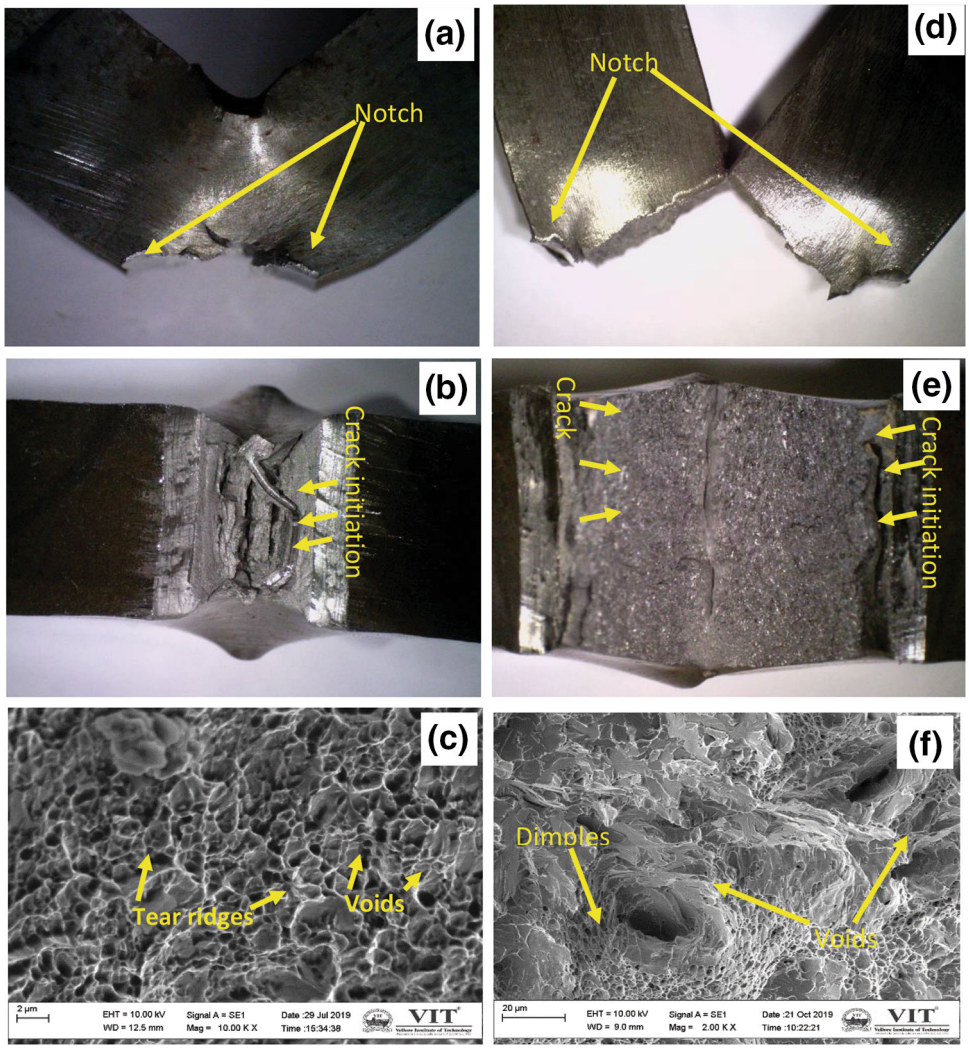

Fig. 16 Fracture impact tested HLAW-2 sample (a-c) at room temperature (d-f) at -60°C (a, c) Side view (b, e) Top view Fractography at 10 KX (f) Fractography at 2 KX

Table 6 Weld chemical composition

Wt%	C	Mn	Si	P	S	Ni	Cr	Mo	V	Cu	Al	Nb	Ti	Pb	Sn	O	N	Fe
HLAW-1	0.096	1.02	0.26	0.018	0.013	2.01	0.024	0.005	0.04	0.146	0.04	0.01	0.02	0.04	0.002	0.02	0.002	Bal.
HLAW-2	0.078	1.4	0.21	0.013	0.016	1.82	0.017	0.001	0.02	0.1	0.11	0.014	0.006	0.16	0.004	0.01	0.004	Bal.

Acknowledgments

The authors are thankful to the Naval Research Board (NRB), New Delhi. Project No. NRB-386/MAT/16-17, for providing financial assistance to carry out the project. The authors would like to thank ARCI, Hyderabad, for providing a hybrid laser arc welding facility and support to conduct the experiment.

References

1. S. Mallik, B.S. Minz and B. Mishra, Production of DMR 249A Steel at SAIL, Bokaro Steel Plant, *Adv. Metall. Mater. Manuf. Processes Strateg. Sect.*, 2012, **710**, p 149–154
2. R. Pamnani, M. Vasudevan, T. Jayakumar, P. Vasantharaja and K.C. Ganesh, Numerical Simulation and Experimental Validation of Arc Welding of DMR-249A Steel, *Def. Technol.*, 2016, **12**(4), p 305–315. https://doi.org/10.1016/j.dt.2016.01.012
3. R. Pamnani, M. Vasudevan, T. Jayakumar and P. Vasantharaja, Development of Activated Flux, Optimization of Welding Parameters and Characterization of Weld Joint for DMR-249A Shipbuilding Steel, *Trans. Indian Inst. Met.*, 2017, **70**(1), p 49–57. https://doi.org/10.1007/s12666-016-0857-0

4. M. Sabzi and S.M. Dezfuli, Drastic Improvement in Mechanical Properties and Weldability of 316L Stainless Steel Weld Joints by Using Electromagnetic Vibration During GTAW Process, *J. Manuf. Processes*, 2018, **33**, p 74–85. https://doi.org/10.1016/j.jmapro.2018.05.002
5. S.H. Mousavi Anijdan, M. Sabzi, M. Ghobeiti-Hasab and A. Roshan-Ghiyas, Optimization of Spot Welding Process Parameters in Dissimilar Joint of Dual Phase Steel DP600 and AISI 304 Stainless Steel to Achieve the Highest Level of Shear-Tensile Strength, *Mater. Sci. Eng. A*, 2018, **726**, p 120–125. https://doi.org/10.1016/j.msea.2018.04.072
6. S.H. Mousavi Anijdan and M. Sabzi, The Effect of Heat Treatment Process Parameters on Mechanical Properties, Precipitation, Fatigue Life, and Fracture Mode of an Austenitic Mn Hadfield Steel, *J. Mater. Eng. Perf.*, 2018, **27**(10), p 5246–5253. https://doi.org/10.1007/s11665-018-3625-y
7. M. Sabzi, A. Obeydavi and S.H. Mousavi Anijdan, The Effect of Joint Shape Geometry on the Microstructural Evolution, Fracture Toughness, and Corrosion Behavior of the Welded Joints of a Hadfield Steel, *Mech. Adv. Mater. Struct.*, 2018, **2018**, p 1–11. https://doi.org/10.1080/15376494.2018.1430268
8. S.H. Mousavi Anijdan and M. Sabzi, The Evolution of Microstructure of an High Ni HSLA X100 Forged Steel Slab by Thermomechanical Controlled Processing, *Mineral. Metals Mater. Ser.*, 2018 https://doi.org/10.1007/978-3-319-72526-0_14
9. Masoud Sabzi and Mansour Farzam, Hadfield Manganese Austenitic Steel: A Review of Manufacturing Processes and Properties, *Mater. Res Express*, 2019, **1065c2**, p 1–15. https://doi.org/10.1088/2053-1591/ab3ee3
10. I. Bunaziv, S. Wenner, X. Ren, J. Frostevarg, A.F.H. Kaplan and O.M. Akselsen, Filler Metal Distribution and Processing Stability in Laser-Arc Hybrid Welding of Thick HSLA Steel, *J Manuf. Processes*, 2020, **54**, p 228–239. https://doi.org/10.1016/j.jmapro.2020.02.048
11. J. Feng, L. Li, Y. Chen, Y. Tian, Y. Sun, X. Zhang and J. Zhang, Inhomogeneous Microstructure and Fatigue Crack Propagation of Thick-Section High Strength Steel Joint Welded Using Double-Sided Hybrid Fiber Laser-Arc Welding, *Opt. Laser Technol.*, 2021, **134**, p 1–8. https://doi.org/10.1016/j.optlastec.2020.106668
12. H.R. Jafarian, M. Sabzi, S.H. Mousavi Anijdan, A.R. Eivani and N. Park, The Influence of Austenitization Temperature on Microstructural Developments, Mechanical Properties, Fracture Mode and Wear Mechanism of Hadfield High Manganese Steel, *J. Mater. Res. Tech.*, 2021, **10**, p 819–831. https://doi.org/10.1016/j.jmrt.2020.12.003
13. L. Bao, Y. Wang and T. Han, Study on Microstructure-Toughness Relationship in Heat Affected Zone of EQ70 Steel by Laser-Arc Hybrid Welding, *Mater. Charact.*, 2021, **171**(110788), p 1–11. https://doi.org/10.1016/j.matchar.2020.110788
14. W. Liu, J. Ma, M.M. Atabaki, R. Pillai, B. Kumar, U. Vasudevan, H. Sreshta and R. Kovacevic, Hybrid Laser-Arc Welding of 17–4 PH Martensitic Stainless Steel, *Lasers Manuf. Mater. Process.*, 2015, **2**(2), p 74–90. https://doi.org/10.1007/s40516-015-0007-2
15. An experimental study of arc welding parameters for ultimate strength in bending & hardness on DMR 249A & Optimization. *Proceedings of 54th IRF International Conference*, 8th May, 2016, Pune, India, ISBN: 978-93-86083-10-4. pp. 14–18
16. R. Pamnani, M. Vasudevan, P. Vasantharaja and T. Jayakumar, Optimization of A-GTAW Welding Parameters for Naval Steel (DMR 249 A) by Design of Experiments Approach, *Proc. Inst. Mech. Eng. Part L J. Mater. Des. Appl.*, 2017, **231**(3), p 320–331. https://doi.org/10.1177/1464420715596455
17. R. Pamnani, G.K. Sharma, S. Mahadevan, T. Jayakumar, M. Vasudevan and B.P.C. Rao, Residual Stress Studies on Arc Welding Joints of Naval Steel (DMR-249A), *J. Manuf. Process.*, 2015, **20**, p 104–111. https://doi.org/10.1016/j.jmapro.2015.09.004
18. R. Pamnani, T. Jayakumar, R.P. George, A. Balakrishnan, K. Mudali and M. Vasudevan, Electrochemical Corrosion Studies of Base Metals and Welds of Low Carbon Steels Used in Ship Building Industry, *Innov. Corros Mater. Sci. Formerly Recent Patents Corros. Sci.*, 2016, **6**, p 55–64
19. G. Turichin, M. Kuznetsov, M. Sokolov and A. Salminen, Hybrid Laser Arc Welding of X80 Steel: Influence of Welding Speed and Preheating on the Microstructure and Mechanical Properties, *Phys. Proc.*, 2015, **78**, p 35–44. https://doi.org/10.1016/j.phpro.2015.11.015
20. I. Bunaziv, "Optimization of Parameters for Fiber Laser-MAG Hybrid Welding in Shipbuilding Applications," Master's thesis, Lappeenranta University of Technology, Finland, 2013. Retrieved from https://lutpub.lut.fi/
21. L. Subashini, K.V.P. Prabhakar, R.C. Gundakaram, S. Ghosh and G. Padmanabham, Single Pass Laser-Arc Hybrid Welding of Maraging Steel Thick Sections, *Mater. Manuf. Process.*, 2016, **31**(16), p 2186–2198. https://doi.org/10.1080/10426914.2016.1221099
22. H. Kumar, K.V.P. Prabhakar, S. Sam, S.K. Albert, G. Padmanabham, A.K. Bhaduri, T. Jayakumar and E.R. Kumar, Development of Laser Welding Process for Reduced Activation Ferritic Martensitic Steel for Indian Test Blanket Module, *Fusion Sci. Technol.*, 2014, **66**(1), p 192–199. https://doi.org/10.13182/FST13-747
23. P. Gadhe, B. Shanmugarajan and K. Prabhakar, LASER-MIG Hybrid Welding of Thick Plates of Mild Steel in Single Pass, *Indian Weld. J.*, 2012, **45**, p 29
24. T. Jokinen and V. Kujanpää, High Power Nd:YAG Laser Welding in Manufacturing of Vacuum Vessel of Fusion Reactor, *Fusion Eng. Des.*, 2003, **69**(1), p 349–353. https://doi.org/10.1016/S0920-3796(03)00071-1
25. M. Bachmann, A. Gumenyuk and M. Rethmeier, Welding with High-Power Lasers: Trends and Developments, *Phys. Procedia*, 2016, **83**, p 15–25. https://doi.org/10.1016/j.phpro.2016.08.003
26. X. Xu, G. Mi, Y. Luo, P. Jiang, X. Shao and C. Wang, Morphologies, Microstructures, and Mechanical Properties of Samples Produced Using Laser Metal Deposition with 316L Stainless Steel Wire, *Opt. Lasers Eng.*, 2017, **94**, p 1–11. https://doi.org/10.1016/j.optlaseng.2017.02.008
27. J. Lin, N. Ma, Y. Lei and H. Murakawa, Measurement of Residual Stress in Arc Welded Lap Joints by Cosα X-Ray Diffraction Method, *J. Mater. Process. Technol.*, 2017, **243**, p 387–394. https://doi.org/10.1016/j.jmatprotec.2016.12.021
28. B. Białobrzeska, Łukasz Konatand Robert Jasiński, *Influ. Austenite Grain Size Mech. Prop. Low-Alloy Steel Boron Metals*, 2017, **7**, p 26. https://doi.org/10.3390/met7010026
29. Z. Zhang and R.A. [Univ. of S. (United K.D. of M.E. Farrar, Influence of Mn and Ni on the Microstructure and Toughness of C-Mn-Ni Weld Metals, (United States), 1997, https://www.osti.gov/biblio/500906
30. Z. Tang and W. Stumpf, The Role of Molybdenum Additions and Prior Deformation on Acicular Ferrite Formation in Microalloyed Nb–Ti Low-Carbon Line-Pipe Steels, *Mater. Charact.*, 2008, **59**(6), p 717–728. https://doi.org/10.1016/j.matchar.2007.06.001
31. H.-J. Lee and H.-W. Lee, Effect of Cr Content on Microstructure and Mechanical Properties of Low Carbon Steel Welds, *Int. J. Electrochem. Sci.*, 2015, **10**, p 8028–8040
32. R.A. Farrar and Z. Zhang, Aspect Ratios and Morphology of Acicular Ferrite in C-Mn–Ni Weld Metals, *Mater. Sci. Technol.*, 1995, **11**(8), p 759–764. https://doi.org/10.1179/mst.1995.11.8.759
33. S. Babu, "Acicular Ferrite and Bainite in Fe-Cr-C Weld Deposits". Doctoral thesis, University of Cambridge, England, 1991. https://doi.org/10.17863/CAM.14232
34. X.-N. Wang, S.-H. Zhang, J. Zhou, M. Zhang, C.-J. Chen and R.D.K. Misra, Effect of Heat Input on Microstructure and Properties of Hybrid Fiber Laser-Arc Weld Joints of the 800MPa Hot-Rolled Nb-Ti-Mo Microalloyed Steels, *Opt. Lasers Eng.*, 2017, **91**, p 86–96. https://doi.org/10.1016/j.optlaseng.2016.11.010
35. H.R. Jafariana, M. Sabzib, S.H. Mousavi Anijdanc, A.R. Eivania and N. Parkde, The Influence of Austenitization Temperature on Microstructural Developments, Mechanical Properties, Fracture Mode and Wear Mechanism of Hadfield High Manganese Steel, *J. Mater. Res. Tech.*, 2021, **10**, p 819–831. https://doi.org/10.1016/j.jmrt.2020.12.003
36. M. Sabzia and S.M. Dezfulib, Post Weld Heat Treatment of Hypereutectoid Hadfield Steel: Characterization and Control of Microstructure, Phase Equilibrium, Mechanical Properties and Fracture Mode of Welding Joint, *J. Manuf. Processes*, 2018, **34**, p 313–328. https://doi.org/10.1016/j.jmapro.2018.06.009
37. R. Pamnani, T. Jayakumar, M. Vasudevan and T. Sakthivel, Investigations on the Impact Toughness of HSLA Steel Arc Welded Joints, *J. Manuf. Process.*, 2016, **21**, p 75–86. https://doi.org/10.1016/j.jmapro.2015.11.007
38. H.A. Abdullah and R.A. Siddiqui, Concurrent Laser Welding and Annealing Exploiting Robotically Manipulated Optical Fibers, *Opt. Lasers Eng.*, 2002, **38**(6), p 473–484. https://doi.org/10.1016/S0143-8166(01)00174-9

39. A.A. Johnson and R.J. Storey, "The Effect of Carbon on the Charpy V-Notch Ductile-Brittle Transition Curve," *International Conference and Exhibition on Analysis & Testing of Materials*, 2008. Retrieved from https://citeseerx.ist.psu.edu/
40. H. Zhao and E.J. Palmiere, Effect of Austenite Grain Size on Acicular Ferrite Transformation in a HSLA Steel, *Mater. Charact.*, 2018, **145**, p 479–489. https://doi.org/10.1016/j.matchar.2018.09.013
41. J. Pak, J. Jang, H.K.D.H. Bhadeshia and L. Karlsson, Optimization of Neural Network for Charpy Toughness of Steel Welds, *Mater. Manuf. Process.*, 2009, **24**(1), p 16–21